Photoelectron spectroscopy of size-selected transition metal clusters: Fe_n^-, $n=3-24$

Lai-Sheng Wang[a)]
Department of Physics, Washington State University, Richland, Washington 99352 and Environmental Molecular Sciences Laboratory, Pacific Northwest Laboratory, Richland, Washington 99352

Han-Song Cheng
Air Products and Chemicals, Inc., Allentown, Pennsylvania 18195

Jiawen Fan
Environmental Molecular Sciences Laboratory, Pacific Northwest Laboratory, Richland, Washington 99352

(Received 8 November 1994; accepted 21 March 1995)

A higher resolution magnetic bottle photoelectron spectrometer for the study of the electronic structure of size-selected metal clusters is presented. The initial study on Fe_n^- ($n=3-24$) is reported at a photon energy of 3.49 eV. The photoelectron spectra of these clusters exhibit sharp features throughout the size range. The spectra for Fe_{3-8}^- show large size dependence with many resolved features. The spectra for Fe_{9-15}^- exhibit some similarity with each other, all with a rather sharp feature near the threshold. An abrupt spectral change occurs at Fe_{16}^-, then again at Fe_{19}^- and Fe_{23}^-. These photoelectron spectral changes coincide remarkably with changes of the cluster reactivity with H_2. Extended Hückel molecular orbital (EHMO) calculations are performed for all the clusters to aid the spectral interpretations. The calculations yield surprisingly good agreement with the experiment for clusters beyond Fe_9 when body-centered cubic (bcc) structures are assumed for Fe_{9-15} and a similarly close-packed structure with a bcc Fe_{15} core for the larger clusters. The EHMO calculations allow a systematic interpretation of the sharp photoelectron spectral features in Fe_{9-15}^- and reproduced the abrupt spectral change taking place from Fe_{15}^- to Fe_{16}^-. Most importantly, the reactivity changes of the clusters with H_2 are successfully explained based on the detailed electronic structures of the clusters, as revealed from the photoelectron spectroscopy (PES) spectra and the theoretical calculations. The calculations also correctly predict the existence of magnetism in these clusters and yield reasonable values for the cluster magnetic moments.

I. INTRODUCTION

One of the fundamental issues in the study of metal clusters is to understand the electronic structures of these intermediate systems and their evolution toward bulk band structure as the cluster size increases.[1] Of all the metal clusters, transition metal clusters are of particular interest due to their diverse physical and chemical behavior. Unusual physical and chemical properties are expected for these clusters. Some of these clusters are found to be magnetic with significantly higher magnetic moments than in bulk materials.[2–5] Their chemical reactivity is also found to be strongly size-dependent.[6–14] Primarily due to the presence of partially filled *d* orbitals, however, the transition metal clusters have presented considerable challenges theoretically. Even the dimer systems are found to have very complicated electronic structures and the nature of their bonding properties has not been completely understood.[15–21] Heretofore, very little is known about the detailed structures of transition metal clusters and their electronic properties. Two early review articles have summarized the experimental and theoretical aspects of transition metal clusters.[22,23]

One of the most extensively studied transition metal cluster systems is the iron cluster systems. Research on the chemical reactivity of iron clusters reveals a strong size effect.[6–14] In particular, the reactivity of small iron clusters with H_2 exhibits striking size dependency with orders of magnitude variations in reaction rate between sizes 15 and 16, 18 and 19, and, to a less extent, between 22 and 23.[8,9] Because of the unique ferromagnetic properties of bulk iron, studies on the magnetic properties of the small iron clusters have drawn considerable interests. All iron clusters are found to be magnetic with higher moments than those found in the bulk.[2–5] In other experimental aspects, ionization potentials (IPs) (Refs. 24–26) and dissociation energies of the positive clusters[27] have been measured.

Several possible interpretations have been proposed to account for the dramatic size dependency of the chemical reactivity of the iron clusters with H_2. Whetten *et al.* first made the interesting observation between the cluster reactivity and the cluster IPs.[9] Their proposed model for the reactivity involved the cluster-to-hydrogen charge transfer. Subsequently, Siegbahn *et al.* focused on the detailed electronic structure of the clusters on the reactivity and showed that the correlation between the IP and reactivity is only a secondary consequence of the electronic structure of the clusters.[28] Moreover, Richtsmeier *et al.* stressed the geometrical structure effect on the cluster reactivity.[8] Recently, Conceicao *et al.* found that there is a better correlation between the cluster reactivity and the difference of the cluster IP and

a)To whom correspondence should be addressed.

 0021-9606/95/102(24)/9480/14/$6.00

EA.[29] They proposed that the reactivity is determined by an entrance channel barrier, with a magnitude proportional to the (IP−EA) difference.

Theoretically, several studies have attempted to understand the electronic structure of the iron clusters.[30–36] However, the complicated nature of these systems only allows a few selected high symmetry and very small systems to be studied. It is worth mentioning the IP calculations by Pastor *et al.* with a tight-binding method.[33] They systematically treated Fe_n from $n=3$ to 25 and found good agreement with measured IPs by assuming a body-centered cubic (bcc)-type structure for $n \geqslant 9$. *Ab initio* calculations have only been performed for the iron dimer.[19,20,34–36]

Because of the high density of electronic states found in transition metal clusters, conventional laser spectroscopic techniques cannot be applied to these clusters except to dimers and, perhaps, a few trimers. Photoelectron spectroscopy (PES), involving single-photon, nonresonant transitions from the ground state of a size-selected anion cluster to the various states of the neutral cluster, is ideal to probe the electronic structure of clusters.[37–43] We have completed a modified magnetic-bottle time-of-flight (MTOF) PES apparatus with high mass resolution and improved electron energy resolution.[38,44] It is aimed to obtain high resolution PES spectra for a wide range of cluster systems.[45–48] The combination of a laser vaporization cluster source and the high efficiency and higher resolution capabilities of this apparatus will allow many novel clusters to be studied in considerable detail.

In this paper we report the details of the MTOF-PES apparatus and the first PES study on Fe_n^- clusters for $n=3$–24. Well-resolved PES spectra at 3.49 eV photon energy for these clusters are presented. In contrast to the expectation that the high density of states for transition metal clusters would yield broad spectra, we have observed consistent sharp spectral features near the threshold through the whole size range studied. More interestingly, the observed PES spectral variations correspond well with the cluster chemical reactivity changes with H_2, suggesting the importance of the electronic structure to the cluster reactivity. To aid the spectral interpretations and gain insight into the details of the cluster electronic structure, we carry out extended Hückel molecular orbital (EHMO) calculations for all the clusters. Surprisingly, the EHMO results yield qualitative agreement with the experiment. The calculations also provide important insights into the chemical reactivity of the clusters, as well as the cluster magnetism.

The organization of this paper is as follows. In Sec. II, we report the details of our MTOF-PES apparatus, which currently can achieve a mass resolution ($M/\Delta M$) of more than 500 and an electron energy resolution of better than 20 meV at 1 eV electron kinetic energy. We use EHMO theory to calculate the electronic states for a variety of chosen cluster structures. The details of the EHMO calculations are described in Sec. III. The PES spectra of the Fe_n^- cluster for $n=3$–24 are then presented in Sec. IV. The calculated results are used to help interpret the experimental observations. In Sec. V we give further in-depth discussions on the iron cluster electronic structure. We pay particular attention to the cluster chemical reactivity with H_2 and the cluster magnetism. It will be shown how the electronic structure information obtained is used to give a microscopic understanding of the size dependence of the cluster reactivity. Finally, Sec. VI summarizes the conclusions derived from the present work.

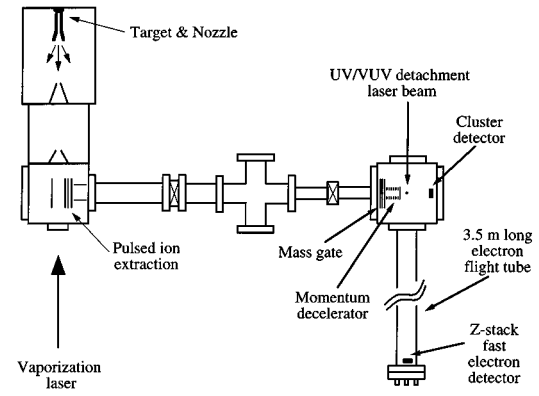

FIG. 1. Schematic view of the laser-vaporization/magnetic-bottle photoelectron spectroscopy apparatus.

II. EXPERIMENT

Figure 1 shows a schematic view of our MTOF-PES apparatus. It consists of a laser vaporization cluster source, a modified Wiley–McLaren time-of-flight (TOF) mass spectrometer, a mass gate, a momentum decelerator, and a MTOF electron analyzer. In the following paragraphs we describe each part in detail.

A. Cluster source

A sufficiently cold and intense negative cluster beam is essential for high resolution PES experiments. Due to the electron attachment energy, negative cluster ions can carry substantial internal energies and are more difficult to cool. We use a large ''waiting room'' nozzle and an intense supersonic expansion to maximize cluster cooling. A drawing of the details of the nozzle is shown in Fig. 2. The vaporization laser beam is directed collinearly with the cluster beam and

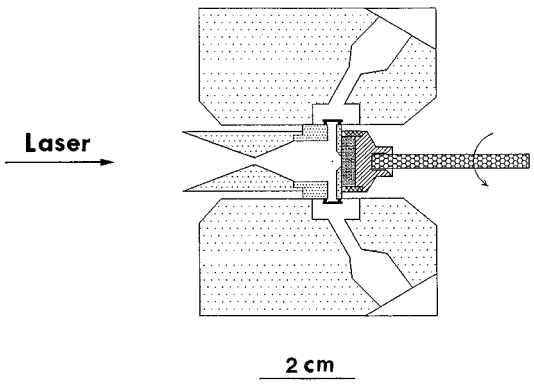

FIG. 2. Schematic cross-sectional view of the large ''waiting room'' laser vaporization nozzle, showing the double Jordan valves and the sample disk assembly.

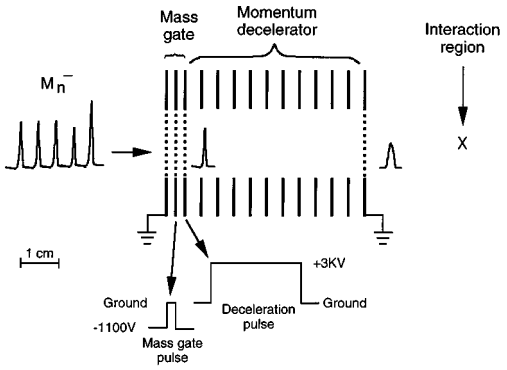

FIG. 3. The mass gate and the momentum decelerator.

hits the target disk after passing the 2 mm nozzle orifice. The laser beam, typically 20 mJ from the second harmonic of a Nd:YAG laser, is focused down to a 1 mm diam spot onto the target. Two pulsed molecular beam valves (R. M. Jordan Co., CA), symmetrically mounted, as shown in Fig. 2, are used to deliver a short and intense helium carrier gas pulse (at 10 atm backing pressure), which mixes with and cools the laser-induced plasma to produce clusters, including both neutral and charged species. The cluster/He mixture undergoes a supersonic expansion and is skimmed twice to form a well-collimated cluster beam into the ion extraction chamber. A liquid-nitrogen-cooled nozzle can be used to supplement the supersonic cooling of the clusters. This is not used in the current experiment. Different nozzle geometries can be used to alter the clustering conditions and cluster cooling. The large waiting room nozzle favors cluster formation and is known to produce colder negative clusters.[49]

B. Mass selection and momentum deceleration

The negative clusters are extracted perpendicularly from the beam by a 1 kV high voltage pulse (EUROTEK, HTS50-21) and are subjected to a TOF mass analysis. The mass spectrometer used is a modified Wiley–McLaren-type, which was first described by de Heer and Milani for large volume ion extraction and simultaneous high mass resolution.[50] The major modification is an addition of a short free-flight zone in between the two acceleration stages of the original Wiley–McLaren design. As shown by de Heer and Milani, this modification can achieve high mass resolution with a large extraction zone appropriate for extracting metal clusters from beams. We have obtained a mass resolution ($M/\Delta M$) of more than 500 at low masses. It deteriorates at higher masses, mainly limited by the fringe field effect due to the ion steering to compensate for the transverse velocity of the clusters. Implementation of a dynamic ion steering system[50] is expected to increase the mass resolution to over 1000.

A three-grid mass gate is used for mass selection as shown in Fig. 3. The first and third grids are at ground, and the middle grid is at negative high voltage (-1.1 kV) so that no clusters are able to pass. Once the desired cluster arrives at the first grid, the high voltage is pulsed to ground for a short period allowing the cluster to pass unaffected. A fast transistor switch (EUROTEK, HTS-30GM) is used to deliver sharp and variable width pulses for the mass gate.

Following the mass gate, the selected cluster beam enters a momentum decelerator. Once the cluster packet passes the third grid of the mass gate, a positive square high voltage pulse (EUROTEK, HTS-30GM) is applied to this grid for the momentum deceleration. The high voltage is pulsed to ground before the ion packet leaves the deceleration stack, which consists of ten guarded rings to ensure a uniform deceleration field. Both the pulse amplitude and the pulse width can be varied to achieve the best deceleration effect. All ions experience the same decelerating force within the same time period, thus will be decelerated by the same amount of linear momentum. Markovich *et al.* first used this deceleration strategy in their MTOF-PES apparatus and have shown that it works quite effectively.[51]

The large volume ion extraction imparts a substantial amount of initial energy spread on the cluster beam, making the usual retarding field deceleration very ineffective.[38] The momentum decelerator not only allows more deceleration, but also yields less ion spread. In contrast to the retarding field deceleration where the ion energy distribution does not change after the deceleration, the final ion energy distribution after the momentum deceleration is reduced approximately as the following for a mass selected cluster packet:

$$\Delta E_f = (E_f/E_i)^{1/2}\Delta E_i, \tag{1}$$

where E_i and ΔE_i are the initial ion mean kinetic energy and the initial ion energy distribution, and E_f and ΔE_f are the final ion mean energy and energy distribution after the momentum deceleration, respectively. As will be shown below, this deceleration step is crucial to improve the MTOF electron energy resolution due to the minimization of the Doppler broadening.

Figure 4 illustrates the working of the mass gate and the momentum deceleration. Figure 4(a) shows the mass spectrum of Cu^+ from laser vaporization of a Cu target. The two isotopes of Cu are well-resolved. Each peak has a width (FWHM) of about 35 ns, yielding a mass resolution of about 480. Figure 4(b) shows the mass selected $^{65}Cu^+$ isotope peak, while Fig. 4(c) shows the decelerated $^{65}Cu^+$ peak by a 2 kV, 550 ns wide pulse. The ions after the deceleration have a mean energy of about 30 eV in this case, compared to 1000 eV initial beam energy with a roughly 10% spread. There is still moderate beam spread after the deceleration as shown in Fig. 4(c). However, this represents the spread at the detector that is much further down stream from the decelerator. At the interaction zone, only 3 cm away from the decelerator, the beam spread should be much better. Furthermore, the beam spread will be much less severe for heavier clusters due to the smaller velocity distribution.

C. Magnetic-bottle time-of-flight photoelectron spectrometer

The magnetic-bottle type of TOF photoelectron spectrometer first described by Kruit and Read[44] is ideal for the study of clusters due to its high collecting efficiency (2π solid angle), which compensates for the low cluster number density. This design has since been implemented for negative

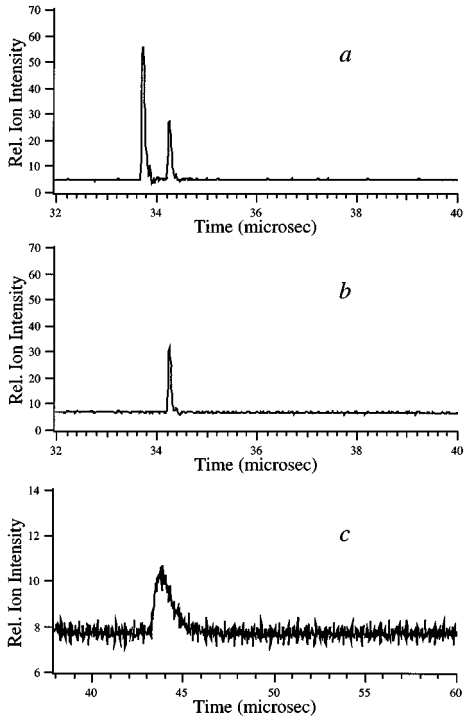

FIG. 4. (a) Mass spectrum of Cu^+ from laser vaporization of a Cu disk, showing the two well resolved isotopes of Cu (^{63}Cu, 69%, and ^{65}Cu, 31%). The mass resolution here is $M/\Delta M=480$. (b) Mass-selected $^{65}Cu^+$ isotope peak. (c) Decelerated $^{65}Cu^+$ isotope peak with a high voltage pulse (2 kV pulse height, 550 ns pulse width).

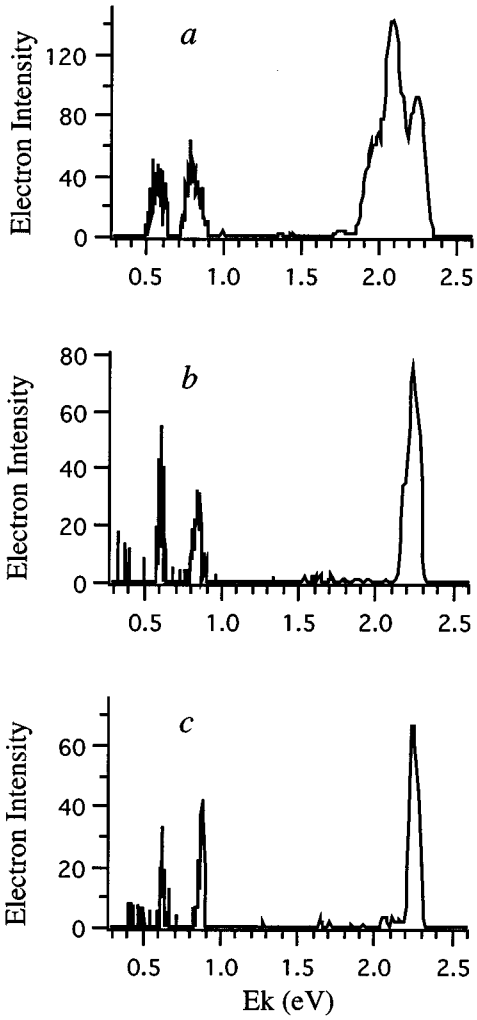

FIG. 5. Photoelectron spectra of Cu^- at 3.49 eV photon energy showing the effect of ion deceleration on the photoelectron energy resolution. Deceleration pulse (a) 2 kV, 200 ns; (b) 2 kV, 400 ns; (c) 2 kV, 600 ns.

cluster studies and configured to collect all 4π solid angles.[38,39] Our apparatus is a modified 4π version of the MTOF, using a pulsed electromagnet for the high field ($\sim$500 G). This externally mounted magnet allows ultrahigh vacuum conditions (10^{-10} Torr) to be obtained in the electron detachment zone.[38]

As shown in Fig. 1, the MTOF is located at the end of the TOF mass spectrometer. The detachment zone is 3 cm downstream from the momentum decelerator. A set of in-line microchannel plates, about 12 cm down from the detachment zone, is used as the cluster mass detector. The MTOF tube is 3.5 m long, at the end of which is located a fast Z-stack electron detector. Not shown in the figure are the high field external electromagnet, and the low field solenoid and the double μ-metal shielding along the 3.5 m MTOF tube.

As mentioned above, the Doppler broadening is a serious resolution limiting factor for the MTOF due to the initial ion kinetic energy. Since photoelectrons are collected from all 4π solid angles, the electrons acquire a maximum velocity spread of $2v$ in the laboratory frame as a result of the finite parent ion velocity, v. The resultant electron energy spread can be expressed as

$$\Delta E_e=4[(m_e/m)(E_eE)]^{1/2}, \tag{2}$$

where E_e and E are the kinetic energies of the photoelectrons and the parent negative cluster ions, respectively, while m_e and m are the corresponding masses. Figure 5 shows the effect of the cluster deceleration on the electron energy resolution of Cu^- at 3.49 eV photon energy. The spectra show the transitions from the ground state of Cu^- ($^1S_0,3d^{10}4s^2$) to the ground state of Cu ($^2S_{1/2},3d^{10}4s^1$) and the first two excited states of Cu ($^2D_{5/2}$ and $^2D_{3/2}$, $3d^94s^2$).[52] The bottom panel shows a deceleration of the Cu^- with a 2 kV and 600 ns pulse. The Cu^- ions have a mean kinetic energy of less than 10 eV. The ^2S peak has a FWHM of 50 meV, and the two excited state peaks have a FWHM of about 30 meV. Further deceleration of the Cu^- does not improve the resolution any more, suggesting that this resolution is no longer limited by the Doppler broadening. We have demonstrated that by simply replacing the high field electromagnet with a permanent magnet (yielding $\sim$700 G at the interaction region) about 20 meV resolution can be achieved at 1 eV electron kinetic energy.[53] Even better resolution is expected at lower electron kinetic energies (Ek) since the resolution (ΔE) varies as $(\mathrm{Ek})^{3/2}$. Cha *et al.* also achieved impressive resolution in a similar MTOF PES apparatus by using essentially a retarding field deceleration method, which works well in their case primarily due to the very low extraction voltage used.[43]

Oxide contamination is known to be a serious problem in laser vaporization generation of metal clusters. There are three major oxygen sources; (1) oxide layer on the target surface; (2) trace amount of oxygen impurity in the carrier gas; and (3) adsorbed water and oxygen on the interior walls of the gas lines and the pulsed molecular beam valves. To minimize the problem, we use ultrahigh purity He (99.9999%) as the carrier gas with an inline liquid nitrogen trap. Before each experiment, the gas lines and the pulsed valves are fully baked with He flushing to desorb any water and oxygen. The target surface oxide layer can be substantially reduced after the target is laser ablated several times. With these measures, the Fe_nO^- signals are reduced to less than 5% of the pure clusters and they are diminished after continuous use of the target. For n up to 8 we could separate the pure clusters from the oxide clusters completely. However, due to the 5.8% natural abundance of ^{54}Fe, the Fe_nO^- peak would overlap with the pure clusters for n larger than 8. We estimate the Fe_nO^- contamination is no more than 1% in the worst case. Using an O_2/He mixed carrier gas, we have studied Fe_nO^- clusters for n up to 16, which are interesting in their own right.[48]

The PES spectrum of Cu^- is used for the spectrometer calibration. All the PES spectra of the Fe_n^- clusters are taken at comparable resolution as that of the best Cu^- spectrum, as shown in Fig. 5(c). The iron clusters are heavier than the Cu atom and can be decelerated more easily than the Cu^- anion since the heavier ions have narrower velocity distributions. The third harmonic of a Nd:YAG laser (3.49 eV) is used for the detachment. Each spectrum is averaged with between 30 000 and 60 000 laser shots at 10 Hz repetition rate. The electron kinetic energy spectra are subtracted from the photon energy to obtain the electron binding energy spectra presented.

III. INTERPRETATION OF PHOTOELECTRON SPECTRUM AND EXTENDED HÜCKEL MOLECULAR ORBITAL (EHMO) CALCULATIONS

A. Interpretation of photoelectron spectrum

Photoelectron spectroscopy probes the electronic structure of matter. Photodetachment transitions occur between the ground state of an anion to the ground and various excited states of the corresponding neutral. PES spectra are usually interpreted based on the single electron approximation, where single electron removals from occupied MOs yield the spectral features. Although this approximation is quite crude and ignores relaxation effects, multiplet splittings, and electron correlations, it still provides a useful means to interpret the main PES spectral features and can yield much insight into the molecular bonding and electronic structures. Due to their high numbers of unpaired d electrons, iron clusters have been very difficult to treat theoretically. Several theoretical studies have been performed on the electronic structure of a few selected Fe clusters.[30–36] However, a detailed interpretation of the current PES spectra based on these calculations is not yet possible.

To illustrate the difficulties in treating these systems, it might be instructive to point out that even the electronic structure of the dimer, the only iron cluster that has been well studied, is still not been fully understood. Leopold and Lineberger obtained a beautiful vibrationally resolved PES spectrum of Fe_2^- at 2.540 eV photon energy.[17] In contrast to previous calculations, which predicted Fe_2 would have 112 states within 0.5 eV above its ground state,[16] they only observed two states. This was interpreted to be due to a rather strong $d-d$ interaction.[18] The ground state configuration of the anion was assigned to be $3d^{13}\sigma_{4s}^2\sigma_{4s}^{*2}$ and the two PES features were assigned to be from detachment of a σ_{4s}^* electron either high- or low-spin coupled with the unpaired $3d$ electrons—leading to a $3d^{13}\sigma_{4s}^2\sigma_{4s}^{*1}$ ground state configuration for Fe_2. Two *ab initio* calculations have followed this work, and the most recent calculation yields a $3d^{14}\sigma_{4s}^2$ ground state configuration for Fe_2, in disagreement with the experimental assignment.[19,20] Not surprisingly, there has been no *ab initio* calculation on the iron clusters beyond the dimer.

Therefore, it is a formidable task to interpret the PES spectra of the iron clusters. As a first step to systematically understand the PES spectra and gain better insight into their electronic structure, we have carried out EHMO calculations on all the clusters presented here. The geometrical structures of the clusters are systematically selected except for Fe_{6-8}. The EHMO theory has been used previously to study the structures and bonding of several metal clusters and has been shown to yield reasonable results for alkali clusters.[54–56] We attempt to use the EHMO results as a guide in the spectral interpretation and compare them with other results where available. Despite its simplicity, the EHMO results give qualitative agreement with the current experiment, leading to important insight into the electronic structure of these clusters. Emphasizing the qualitative nature of the EHMO results, we look for insight that can be obtained from these calculations about the complicated electronic structure of the Fe clusters.

B. Extended Hückel molecular orbital calculations

The extended Hückel theory is a semiempirical quantum mechanical method[57] that has considerable success in studying chemisorption phenomena on surfaces and a variety of solid state chemistry and physics problems by Hoffmann and co-workers.[58–60] It provides a simple and heuristic view on many physical and chemical processes in the condensed phase, despite its admitted lack of numerical accuracy.

The EHMO computational procedure can be briefly described as follows. One starts with the Fock equation

$$\mathbf{FC}=\mathbf{ESC}, \tag{3}$$

where **C** denotes the molecular orbital coefficient matrix and **E** is the energy matrix. The overlap matrix **S** can be conveniently calculated from the basis set. In the EHMO scheme, the Fock matrix **F** is defined as the following: its diagonal elements are completely determined by the valence state ionization potentials of the atomic orbitals; the off-diagonal elements are defined by the diagonal matrix elements as well as the overlap matrix elements and interaction matrix elements that are purely empirical parameters. The Fock matrix possesses correct symmetry properties arrived from the given

molecular structures, and the built-in atomic ionization potentials are directly obtained from experimental measurements. Therefore, EHMO theory yields correct symmetry information on the molecular orbitals, and the calculated energy levels usually correlate reasonably well with the molecular ionization potentials. The EHMO scheme normally uses a noniterative procedure. One can solve the Fock equation by direct matrix diagonalization to obtain the molecular orbitals and the energy levels. Thus, computationally, it is highly efficient.

Unfortunately, in the EHMO scheme, there is no repulsive term built into the Fock matrix. As a consequence, the original EHMO theory cannot be used to optimize molecular geometry. Recently, several studies have shown that when the repulsive forces are included, the EHMO theory can yield quite reasonable optimized geometries for a large number of molecules, as well as several cluster systems, while still maintaining its high computational efficiency.[61]

The geometrical structures of the small iron clusters are not known, and they are difficult to obtain both experimentally and theoretically. Riley and co-workers have done extensive work using chemical means to probe the structures of the iron clusters.[12,14,62,63] One noted conclusion is that a bcc closed shell structure is a very likely candidate for Fe_{15}.[12] Polyicosahedral types of structures have been proposed for Fe_{19} and Fe_{23} when saturated with NH_3.[62] For Fe_{3-5} and Fe_{10-15}, several calculations have been performed, and their geometries optimized.[35,36,64] Interestingly, calculations of the IPs by assuming bcc-type structures for $n \geqslant 9$ yield reasonable agreement with the measured IPs.[33]

In the present calculations, we choose the cluster geometrical structures based on this limited previous knowledge. In particular, we choose the bcc structure for Fe_{9-15}, encouraged by the work of the IP calculations[33] and the experimental indication about the bcc structure for Fe_{15}.[12] Beyond Fe_{15}, we use a close-packed structure based on the bcc Fe_{15} core. For Fe_{3-5}, we use the most recent results from density functional calculations.[36] In some cases, several structures are tested.

In the EHMO scheme, the $3d$, $4s$, and $4p$ of Fe are taken as valence orbitals, of which the $4s$ and $4p$ are represented with a set of single zeta basis functions and the $3d$ with double zeta basis functions. For each cluster, we obtain a set of electronic energy levels and the corresponding molecular orbitals at a given geometry. A central issue is the assignment of the electron occupancy in these levels. While the lower levels are doubly occupied, the occupancy in the upper levels may be singlet, depending on the specific energy level structures. For the iron clusters, the highest occupied molecular orbital (HOMO) and the lowest unoccupied molecular orbital (LUMO) would be nearly degenerate if all electrons were paired in the occupied orbitals. Therefore, according to the Hund's rule,[65] the electron pairs in the upper levels are broken into singly occupied levels; the excess electrons are then transferred into the higher energy levels until an apparent energy gap (0.5 eV or larger) is encountered. This is natural to do since it lowers the electron-electron repulsion due to the exchange energy.[65] In doing so consistently, we obtain a set of occupied energy levels for each cluster with numerous unpaired electrons; thus, the magnetism in these clusters is ''naturally'' revealed. The same effect (i.e., the exchange interaction) produces magnetism in bulk metals.[65]

TABLE I. The numbers of unpaired electrons in the iron clusters obtained from the EHMO calculations. The average magnetic moment (μ_B) is given in the parentheses.

Fe_3	8(2.67)	Fe_{14}	30(2.14)
Fe_4	10(2.50)	Fe_{15}	32(2.13)
Fe_5	12(2.40)	Fe_{16}	36(2.25)
Fe_6	14(2.33)	Fe_{17}	38(2.23)
Fe_7	16(2.28)	Fe_{18}	42(2.33)
Fe_8	18(2.25)	Fe_{19}	46(2.42)
Fe_9	20(2.22)	Fe_{20}	48(2.40)
Fe_{10}	22(2.20)	Fe_{21}	50(2.38)
Fe_{11}	24(2.18)	Fe_{22}	52(2.36)
Fe_{12}	26(2.17)	Fe_{23}	54(2.35)
Fe_{13}	28(2.15)	Fe_{24}	56(2.33)

The numbers of unpaired electrons from the EHMO calculations are listed in Table I. The structures of these clusters that are used are shown in Figs. 6–10. The occupied energy levels, according to their degeneracy and electron occupancy, are plotted as stick spectra in Figs. 6–10 by aligning the HOMO with the threshold features in the experimental PES spectra.[66]

IV. RESULTS AND SPECTRAL INTERPRETATION

The PES spectra of Fe_n^- ($n=3$–24) are shown in Figs. 6–10 with the EHMO occupied energy levels plotted as the stick spectra. The cluster structures used in the EHMO calculations are also shown in the figures. Our results for Fe_{9-16}^- have been reported briefly before.[67] The weak features at the low binding energy side, common to all the spectra, are due to hot band transitions or minor isomers with low electron affinities (EAs) since their intensity varies with the cluster source conditions while the main features remain the same. Well-resolved spectral features are shown for the small clusters, and they are quite different from each other, indicating the molecular nature of the small clusters. The spectra of the larger clusters get increasingly diffuse and they seem to show certain systematic changes. One of the most striking features in the spectra is the sharp peak near the threshold for Fe_{9-15}^-, in particular, Fe_{13}^- to Fe_{15}^-, and the abrupt spectral changes occurring from Fe_{15}^- to Fe_{16}^-. The spectra from Fe_{16}^- to Fe_{18}^- are similar—the small feature appearing in the Fe_{16}^- spectrum seems to increasingly gain intensity in Fe_{17}^- and Fe_{18}^-. In Fe_{19}^-, this small feature becomes a well-resolved peak, and at the same time the whole spectrum shifts to lower binding energy. This pattern seems to repeat from Fe_{20}^- to Fe_{23}^-, where a well-resolved threshold peak appears and the spectrum is again shifted to a lower binding energy. Interestingly, these spectral pattern changes coincide exactly with the chemical reactivity changes of the iron clusters.[8]

The first spectroscopic information obtained from the spectra is the EA of the clusters and its size evolution. There are two definitions of the EA; the vertical EA is the transition energy from the ground state of the anion to the neutral

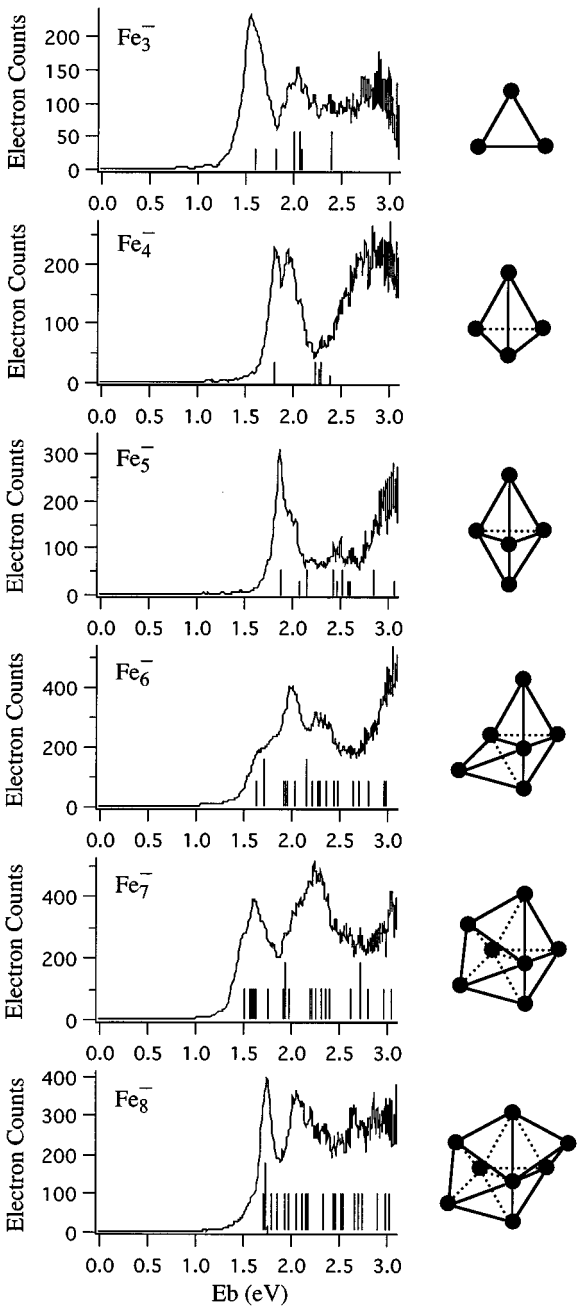

FIG. 6. Photoelectron spectra of Fe_3^- to Fe_8^- at 3.49 eV photon energy. The stick spectra are the occupied energy levels from the extended Hückel molecular orbital calculations by aligning the highest occupied level(s) with the experimental threshold feature. The stick height is proportional to the orbital degeneracy and occupancy. The assumed structures for the corresponding calculations are also shown.

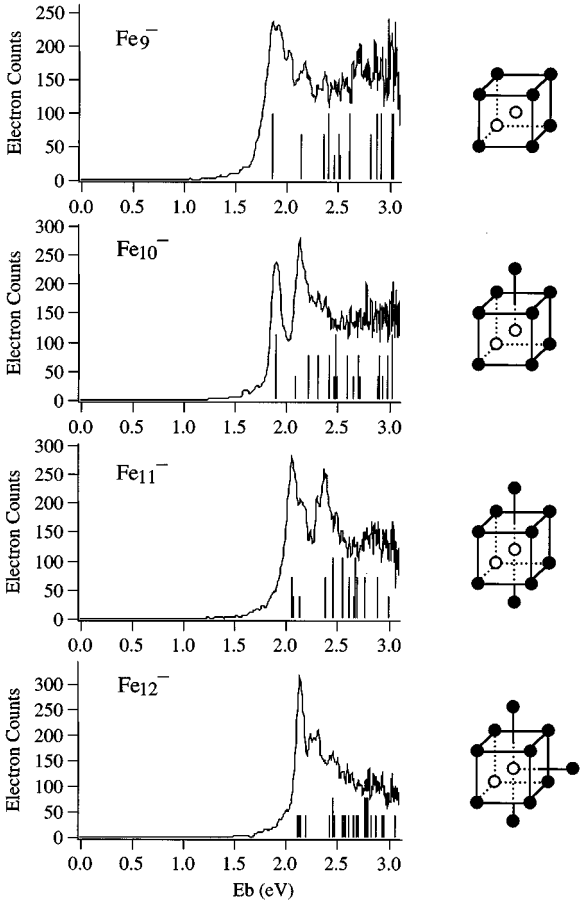

FIG. 7. Photoelectron spectra of Fe_9^- to Fe_{12}^- at 3.49 eV photon energy. See also caption in Fig. 6.

ground state at the same nuclear configuration; the adiabatic EA is the 0–0 transition energy from the anion to the neutral. In the absence of resolved vibrational structures, the adiabatic EA cannot be determined accurately. The vertical EA can be obtained from the peak maxima of the first PES feature. However, even the latter cannot be determined accurately when there are broad and overlapping features near the threshold such as seen in Fe_6^- and Fe_7^-. Therefore, to facilitate comparisons of the EA change as a function of cluster size and to be systematic and consistent, we use the following procedure to estimate the adiabatic EA. Draw a straight line along the slope of the threshold feature and find the binding energy value where this line is crossed with the binding energy axis. This value plus a constant value of 0.07 eV (this accounts for the finite thermal excitations and instrumental resolution) is taken to be the adiabatic EA. The EAs obtained in this manner for the iron clusters are listed in Table II and plotted in Fig. 11. We generously assign an error bar of 0.08 eV although the EAs can be more accurate when sharp features appear at the threshold.

A. Fe_3–Fe_8

1. Fe_3

The spectrum of Fe_3^- shown in Fig. 6 is more complicated than that of Fe_2^-.[17] Beside the two well-separated bands at the lower binding energies, there are more unresolved transitions at the high binding energy side. The most recent local spin density approximation (LSDA) calculation by Castro and Salahub suggests an equilateral triangular structure for Fe_3 with a bond length of 2.10 Å.[36] Using the same structural parameters, we performed EHMO calculations that yielded eight unpaired electrons in agreement with the LSDA calculations. The energy level diagram from the current calculations is displayed in Fig. 12. Note the large

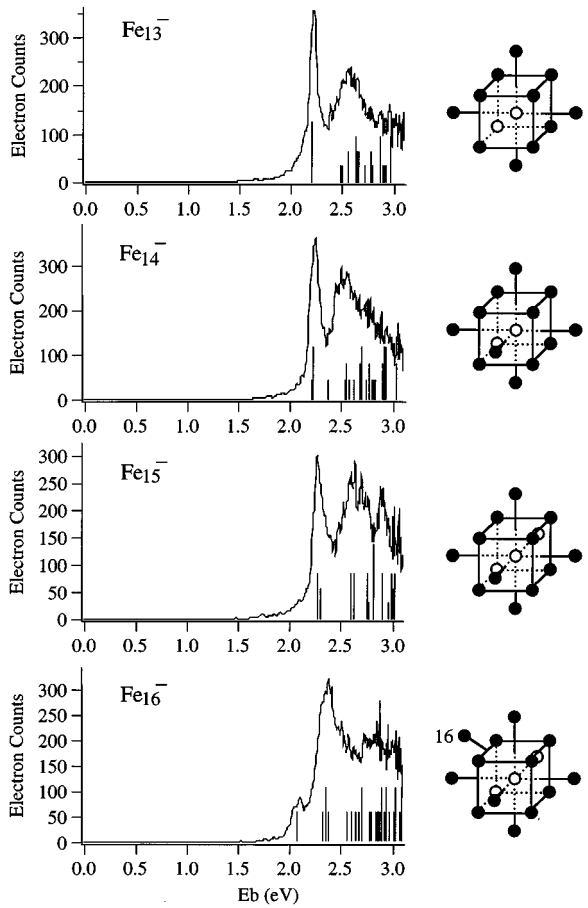

FIG. 8. Photoelectron spectra of Fe_{13}^- to Fe_{16}^- at 3.49 eV photon energy. See also caption in Fig. 6.

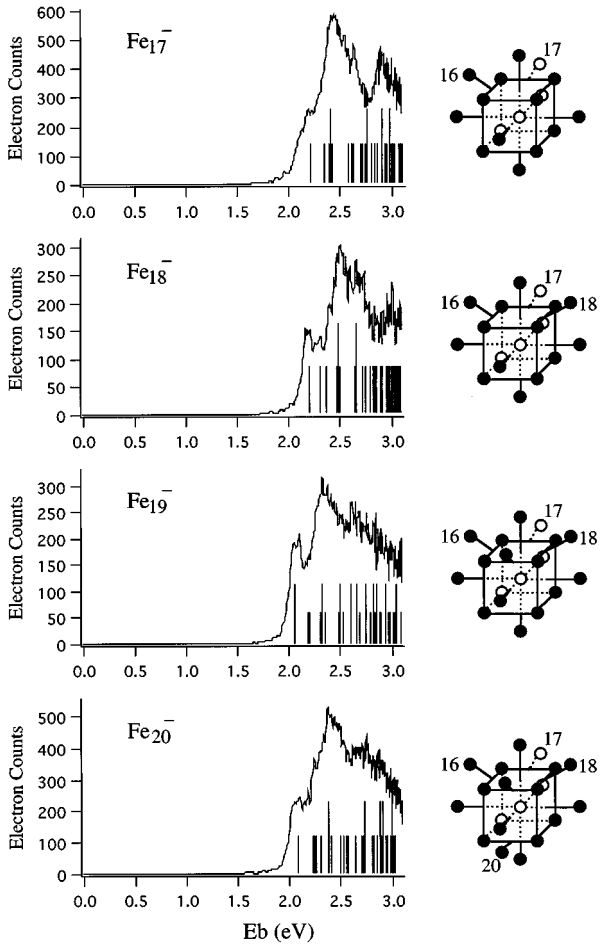

FIG. 9. Photoelectron spectra of Fe_{17}^- to Fe_{20}^- at 3.49 eV photon energy. See also caption in Fig. 6.

gap between the $1a_2'$ and $4e'$ orbitals. If all the electrons were paired, the HOMO-LUMO gap would be between the $3e'$ and $2e''$ orbitals, which are nearly degenerate.

Those occupied levels within the experimental spectrum range are plotted in Fig. 6 as the stick spectrum by aligning the HOMO level with the threshold peak. The HOMO, $1a_2'$, is mostly composed of $3d$ orbitals. The $1a_1''$ orbital is a strong bonding orbital from the $4s$. We assign the first two bands in the spectrum to be from these two orbitals, respectively. In particular, the broad width of the second band agrees with its being from a strong bonding orbital. There are reproducible fine structures on both of these two bands. However, the insufficient resolution plus the seemingly irregular spacing prevents a vibrational assignment. Since Fe_3 has a degenerate ground state in the equilateral triangular structure, it is likely to be Jahn–Teller active, which will further complicate the spectrum. It can be seen from Fig. 6 that there is qualitative agreement between the one-electron EHMO energy levels and the PES spectrum except that the spacings of the calculated levels are too close.

2. Fe_4

The spectrum of Fe_4^- shows two broad and well-separated bands. The second band is limited by the photon energy used and the spectrometer transmission while the first band exhibits a splitting as well as other unresolved fine features. The most recent calculation by Castro and Salahub yields a tetrahedral structure for the cluster with a bond length of 2.22 Å and twelve unpaired electrons.[36] We use the structural parameters obtained by Castro and Salahub in our EHMO calculations, which are shown in Fig. 6 as the stick spectrum, displaying those occupied orbitals in the same energy range as the experiment. The EHMO calculation gives ten unpaired electrons, compared with twelve obtained by Castro and Salahub from their LSDA calculation.

Figure 13 shows the EHMO energy level diagram, which displays two groups of orbitals near the HOMO; a triply degenerate $2t_1$ orbital followed by the densely spaced second group ($3t_2$, $2e$, $1t_1$, and $2a_1$). We assign the first PES band to be from the removal of a $2t_1$ electron and the second band to be from the second group of orbitals. Thus, the EHMO calculation can qualitatively account for the experimental PES spectrum with a tetrahedral structure. The tetrahedral Fe_4 cluster has a degenerate ground state, suggesting it is Jahn–Teller active. This is evident from the broad width and the splitting of the first band in the PES spectrum.

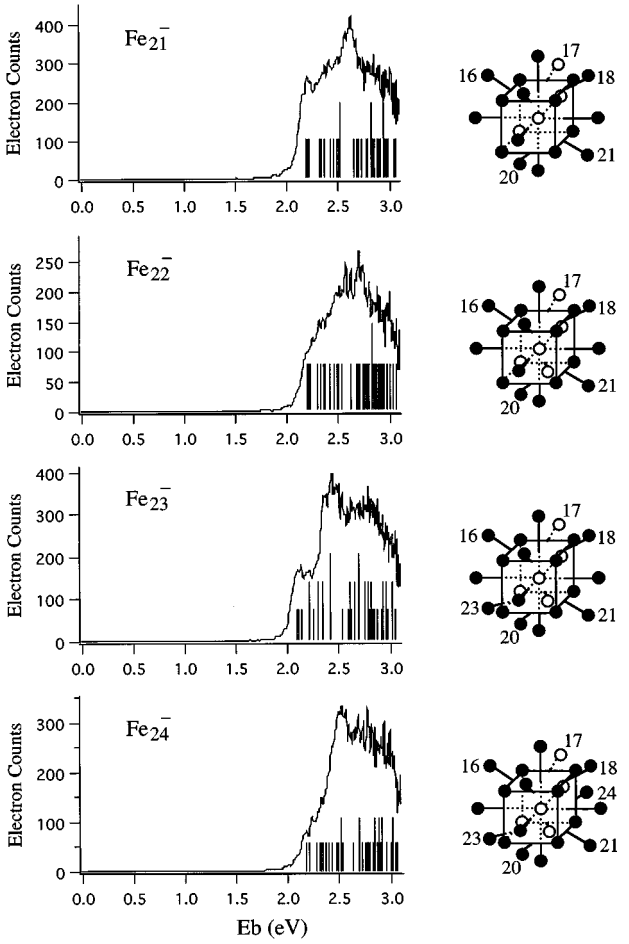

FIG. 10. Photoelectron spectra of Fe_{21}^- to Fe_{24}^- at 3.49 eV photon energy. See also caption in Fig. 6.

3. Fe_5

The spectrum of Fe_5^- displays a sharp peak at the threshold. The spectral pattern looks similar to that of Fe_4^- except that there are weak features between the gap of the two strong bands. The LSDA calculation suggests that a Jahn–Teller distorted bipyramid is the most stable structure for Fe_5.[36] We performed EHMO calculations with the LSDA optimized parameters and obtained rather unsatisfactory results compared to the experiment. Consequently, we tried two other structures; a symmetric bipyramid and a square pyramid. We found that the symmetric bipyramid gives the best result, which is shown in Fig. 6 as the stick spectrum. The calculation does indicate that there are more levels between the first occupied level and the more densely spaced levels at higher binding energy. The sharpness of the PES feature for Fe_5^- suggests that the Jahn–Teller effect in Fe_5 may be rather small if it takes place.

TABLE II. Electron affinities of the iron clusters.[a]

n	EA(eV)	n	EA(eV)
3	1.47(8)	14	2.23(8)
4	1.72(8)	15	2.25(8)
5	1.81(8)	16	2.01(8)
6	1.51(8)	17	2.06(8)
7	1.39(8)	18	2.14(8)
8	1.66(8)	19	2.01(8)
9	1.75(8)	20	2.01(8)
10	1.85(8)	21	2.11(8)
11	2.00(8)	22	2.15(8)
12	2.12(8)	23	2.04(8)
13	2.20(8)	24	2.13(8)

[a]The adiabatic EAs. See Sec. IV for the threshold determination.

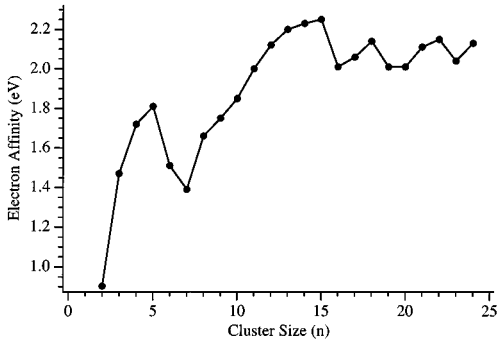

FIG. 11. Electron affinities of the iron clusters as a function of cluster size (n) for $n=2$–24 ($n=2$ from Ref. 17).

4. Fe_{6-8}

For clusters with size larger than Fe_5, there is no calculation intending to optimize the cluster geometries. Therefore, the structural parameters are all assumed in our EHMO calculations. The nearest neighbor internuclear distance used for all the higher clusters is 2.43 Å, compared to the bulk lattice constant of 2.87 Å. The increase of the number of

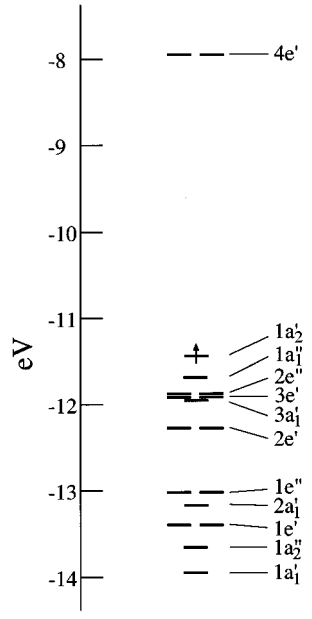

FIG. 12. The extended Hückel molecular orbitals for Fe_3. The arrow indicates the highest occupied level.

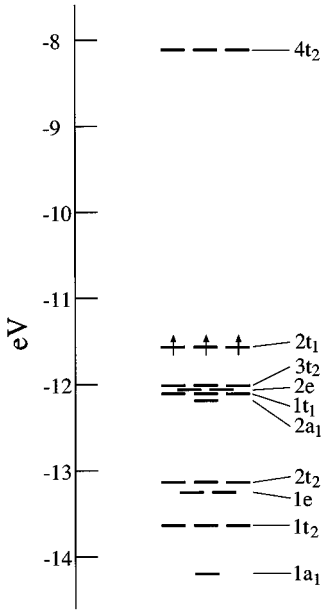

FIG. 13. The extended Hückel molecular orbitals for Fe_4. The arrows indicate the highest occupied levels.

atoms in the clusters also means that there are more possible structures. For each of these clusters we performed EHMO calculations in several geometries.

The spectrum of Fe_6^- shows rather broad features near the threshold, suggesting that there is significant structural change from the anion to the neutral or that there is a strong Jahn–Teller effect. We carried out EHMO calculations in three geometries; octahedron (I), pentagonal pyramid (II), and capped trigonal bipyramid (III, shown in Fig. 6). None of the structures gave satisfactory agreement with the experiment. The stick spectrum shown in Fig. 6 is the EHMO result of structure III. The densely spaced levels illustrate the complexity of this cluster. The diffused features of Fe_6^- are also unusual compared to its neighbors.

The spectrum of Fe_7^-, like that of Fe_6^-, is also lack of sharper features as seen in the other clusters. However, the first band in the Fe_7^- spectrum shows unresolved features, indicating the energy levels are more congested. The results from EHMO calculations, by assuming a pentagonal bipyramid structure, are plotted in Fig. 6 as the stick spectrum. It shows rather congested levels, consistent with the experiment. Both Fe_6 and Fe_7 have rather low electron affinities compared with their neighbors (as is evident in Fig. 11).

The spectrum of Fe_8^- displays a rather sharp feature at the threshold. Previous IP calculations have assumed a cubic structure for Fe_8.[33] We tested three structures in our EHMO calculations; cubic (I), capped pentagonal bipyramid (II, shown in Fig. 6), and a bcc fragment (III) by removing a corner atom of a bcc Fe_9 (see below). None of the calculations yielded satisfactory results. The stick spectrum plotted in Fig. 6 is obtained from structure II, as shown. From its appearance, the spectrum of Fe_8^- is similar to those of the larger clusters. As will be shown below, EHMO calculations, by assuming simple bcc structures, yield rather good agreement for the larger clusters. However, the structure III for Fe_8, which is similar to those bcc structures, gives quite poor agreement with the experiment.

The EHMO calculations do not yield satisfactory interpretations of the PES spectra for these three clusters. This is not surprising since their structural parameters are not known at all. The unusually diffuse spectra of Fe_6^- and Fe_7^- suggest that they may have strong Jahn–Teller effects. The sharp feature in Fe_8^- implies that it should have a rather high symmetry.

B. Fe_9–Fe_{15}

We briefly reported our results on Fe_{9-16}^- previously.[67] For completeness, we present them here and focus on those aspects that could not have been included in the previous discussion. One of the most striking features in the PES spectra of this size range is the sharp features exhibited for all these spectra and their close similarity, as shown in Figs. 7 and 8. Particularly, the sudden spectral change from Fe_{15}^- to Fe_{16}^- coincides exactly with their chemical property changes. On the basis of the various previous structural hints, we use the bcc structure for Fe_{9-15} in our EHMO calculations.[12,33]

The EHMO results for these clusters are plotted in Figs. 7 and 8. For the simplicity of these calculations, the agreement is impressive. The sharp threshold features are especially well accounted for. All these spectra show a gap followed by a broad spectral feature. This is well reproduced by the EHMO calculations. We attribute this good agreement to the correct structural assumptions.

Upon inspecting the EHMO wave functions, we find that all the MOs are fairly delocalized. In particular, the HOMOs of these clusters, which are responsible for the sharp features near the threshold, are all predominantly composed of $3d$ orbitals. Further more, these HOMOs all have the largest d contributions from the central atom in the bcc clusters. These d orbitals from the central atom overlap fairly well with orbitals from the other atoms. The orbital delocalization indicates that the cluster electronic properties as well as their chemical/physical properties might be sensitive to local structure changes, such as that taking place from Fe_{15} to Fe_{16}. It is also significant to observe that the major d contributions to the HOMOs are from the bcc central atom. This plus the structural similarity among these clusters explains the similarity of the cluster PES spectra in this size range. It is worthwhile to point out that the striking similarity among the spectra of Fe_{13}^- to Fe_{15}^- strongly suggests their structural similarity. The bcc structures are the most consistent with this observation.

C. Fe_{16}–Fe_{24}

The Fe_{16}^- spectrum is shown in Fig. 8 along with Fe_{13-15}^- to emphasize the abrupt spectral change from Fe_{15}^- to Fe_{16}^-. The spectra of Fe_{17-24}^- are displayed in Figs. 9 and 10. In the Fe_{16}^- spectrum, a new feature appears at the threshold. Except the new feature in the PES spectrum of Fe_{16}^-, other spectral features are quite similar to those of Fe_{15}^-, and the sharp threshold feature observed in Fe_{15}^- becomes the second band in Fe_{16}^-. The new feature observed in Fe_{16}^- persists in the

higher clusters and seems to gain intensity as the cluster size increases until Fe_{19}^-, where it becomes a distinct sharp feature and at the same time the electron affinity becomes smaller. Although less dramatic compared to the spectral change from Fe_{15}^- to Fe_{16}^-, the PES spectral change from Fe_{18}^- to Fe_{19}^- is significant. From Fe_{19}^- to Fe_{22}^-, the first feature near the threshold becomes less sharp and the EA increases steadily until Fe_{23}^-. Then, as seen before, a rather abrupt sharp feature appears and the EA becomes smaller. The PES spectral changes, taking place from Fe_{18}^- to Fe_{19}^-, and Fe_{22}^- to Fe_{23}^-, as well as from Fe_{15}^- to Fe_{16}^-, correlate remarkably well with the chemical reactivity changes of the clusters with H_2, on which we will give an in-depth discussion later.

It seems that there is a four-atom periodic variation in the PES spectral pattern, from Fe_{16} to Fe_{19} and from Fe_{19} to Fe_{23}. This leads us to suspect that the cluster growth after the bcc Fe_{15} proceeds with a closely packed route; each additional atom attaches to a cubic edge around an apex atom of Fe_{15}. There are 12 such positions. At every fourth atom (i.e., Fe_{19} and Fe_{23}), a rather high symmetry cluster is recovered, consistent with the sharp PES spectral patterns observed for Fe_{19}^- and Fe_{23}^-. It is important to point out that these structures are different from the exclusive bcc structures used in the previous IP calculations.[33]

We perform the EHMO calculations for these clusters using the structures described above. The results are displayed in Figs. 8–10 as stick spectra. The agreement between the calculated energy levels and the PES spectral patterns is rather good, particularly below $n=20$. Quite impressively, the extra feature in Fe_{16}^- is well reproduced. Two other structures for Fe_{16}, a true bcc fragment and one with atom-16 attached to a cube corner of the bcc Fe_{15}, yield quite different energy levels. As the cluster size increases, the energy level structures become more complicated and are increasingly difficult to compare with the experimental PES pattern, especially beyond Fe_{20}. This is understandable since there are more structural possibilities for the larger clusters. For Fe_{19} alone, we performed calculations with two additional structures; fcc and polyicosahedral, two alternative structures which have been discussed for Fe_{19}, previously.[62] The resultant energy levels are definitely worse compared to the PES pattern than the one shown in Fig. 9.

Upon inspecting the calculated wave functions, we found that the HOMO of Fe_{16} is composed mainly of *s* orbitals; the orbitals responsible for the second band in the PES spectrum of Fe_{16}^- are mostly of *d* orbitals with considerable contributions from the *d* orbitals of the central atom, similar to the situation found in the first band of Fe_{15}^-. Further examination of the wave functions indicates that as the cluster increases its size from Fe_{15} to Fe_{16}, the HOMO of the former evolves into the second HOMO (HOMO-2) in Fe_{16}, whose HOMO becomes the *s*-like orbital corresponding to the threshold feature of the PES spectrum. As will be discussed in the next section, this abrupt electronic structure change underlies the reactivity changes of the clusters.

As the cluster size continues to increase, the second band remains to be overwhelmingly *d*-like with a significant contribution from the central atom, whose contribution can be traced even to Fe_{24} with its amplitude decreasing as the cluster size increases. On the other hand, the HOMO, while maintaining significantly *s*-like, continues to evolve with increasing participation from the *d* orbitals.

V. DISCUSSION

A. Electronic and geometrical structural evolution

The electronic structure and EAs of the iron clusters exhibit strong size effect. The small clusters display rather well resolved spectral features. Fe_3 and Fe_4 have equilateral triangular and tetrahedral structures, respectively,[35,36] and their main PES features are reasonably accounted for by the EHMO calculations. However, for Fe_{5-8}, higher level calculations are required to interpret their PES spectra; the current EHMO calculations are insufficient probably due to their structural complexity. Fe_6 and Fe_7 have rather low EAs and unusually diffused PES spectra. The EHMO calculations appear to agree better for the larger clusters ($n \geqslant 9$). We believe this is due to the judicious choices of the cluster structures[12,33] and their insensitivity to precise structural parameters.

The density of states as a function of cluster size increases rather rapidly. It is expected that, beyond Fe_{24}, little sharp features will be resolved even at the present instrumental resolution. However, comparing with nickel clusters in the same size range the iron clusters exhibit much more interesting features. This can be attributed to the stronger interactions of the *d* orbitals in the iron clusters, that is already evident in the dimers.[17] While iron dimer yields an interesting and simple PES spectrum with only two bands within 1 eV above the neutral ground state, the nickel dimer spectrum is much more complicated.[68] The nickel trimer[69] also has a much more complicated spectrum than the iron trimer spectrum reported currently.

The reasonable agreement between the EHMO results and the PES spectra beyond Fe_9 suggests that the bcc-type structure from Fe_{9-15}, and the close-packed structure beyond Fe_{15} are highly probable structures. In fact, the PES spectra themselves are already strongly suggestive that a new shell is started at Fe_{16} in the cluster growth and this shell continues to grow for the larger clusters. This is consistent with the conclusions of the IP calculations by Pastor *et al.* for $n=9$–15 although they assumed bcc-like structures even for $n>15$.[33] If proven to be true, this would be highly unusual and interesting since these clusters already have similar structures as the bulk at such small sizes. Parks *et al.*, through their extensive chemical studies, have proposed a bcc structure for Fe_{15}.[12] However, they suggest polyicosahedral structures for Fe_{19} and Fe_{23} when saturated with NH_3.[62] They have observed adsorbate-induced structural changes. Thus, it is highly possible that the bare clusters may have different structures. Therefore, their conclusions are not in conflict with our structural assumptions. A recent simulated annealing calculation concludes that the small iron clusters have high symmetry and rather hollow structures.[64] Since this calculation predicts the wrong ground state structure for bulk Fe (it yields a fcc rather than the bcc structure for Fe), we conclude that higher level calculations are needed to confirm the structures of these clusters.

The ''central atom effect''—the first sharp PES peaks for Fe_{9-15}^- all have large contributions from the central atom $3d$ orbitals—provides an interesting support for the bcc structural assumptions and explains nicely about the seemingly similarities in the clusters with $n \geqslant 9$. Beyond Fe_{15}, the central atom effect manifests itself in the second PES band, and it can be traced up to Fe_{24}. Interestingly, a unrestricted Hartree–Fock calculation, by using a tight-binding Hubbard model on the bcc Fe_{15}, also predicts that the central atom has a large contribution to the density of states near the Fermi level.[34] The spectrum of Fe_8^- is similar to the larger clusters and should be classified with the Fe_{9-15} series. However, the central atom effect cannot be found in Fe_8. Calculations are performed by using a true bcc fragment for Fe_8, in which a corner atom is removed from the bcc Fe_9. The energy levels do not agree well with the experiment as they do for the higher clusters. It is possible that we do not find the right structure for Fe_8 in the EHMO calculations since, with only eight atoms, it cannot form a true bcc fragment. Yet, the sharp feature at the threshold and the overall spectral pattern of Fe_8^- look quite similar to the higher bcc-type clusters.

How big a cluster is a metal has been an interesting question in cluster research. However, the answer may depend on what properties one is interested in. Recent magnetic studies[2] indicate that the cluster magnetic moments approach the bulk limit at a cluster size of approximately 700 atoms for iron.[2] Clearly, the density of states increases rapidly with cluster size. However, even for the largest cluster investigated in the present study (Fe_{24}), there are still recognizable features in its PES spectrum. Recently, Zhao *et al.* have investigated the metal–nonmetal transition in transition metal clusters with close-packed structures.[70] They concluded that the critical size for the metal–nonmetal transition is about 30–50 atoms, and their criterion was that at the critical point the density of states of the cluster exceeds $1/k_BT$. Our instrumental resolution of 30 meV is close to k_BT at room temperature. As mentioned above, up to Fe_{24} we can still resolve features in its PES spectrum. The EHMO energy levels are also less dense compared to $1/k_BT$. These seem to agree with the theoretical predictions. With careful account for the Franck–Condon profiles in the photodetachment process, further PES studies of the larger clusters should be able to quantitatively test the conclusions for the critical sizes of the anticipated metal–nonmetal transition.

B. Iron cluster magnetism, chemical reactivity, and their electronic structure

Two of the most interesting properties of iron clusters are their magnetism and chemical reactivity, which are closely related to their electronic structures. The magnetic properties of the iron clusters have been well studied and they are all shown to be magnetic.[2–4,30–36] The magnetism of these clusters is also well revealed from the EHMO calculations and the number of unpaired electrons obtained from the EHMO calculations, as shown in Table I, are quite reasonable compared with other theoretical calculations.[30–36] The unpaired electrons of these clusters arise from the nature of the EHMO energy level structures and the tendency to reduce the electron repulsion by occupying as many nearly degenerate or closely spaced levels as possible. This is due to the same exchange interaction that gives bulk magnetism.[65] The correct prediction of the magnetism from the EHMO calculations, although not from the first principle, is interesting.

The dramatic size-dependent reactivity of these clusters with H_2 is well known.[8,9] Several interpretations have been advanced,[8,9,28,29] but it is still not well understood. The central question in interpreting the size-dependent reactivity of these clusters is why the change of only one atom can affect the cluster reactivity so dramatically.

In the present study, we intend to show that the iron cluster chemical reactivity with H_2 can be best described by considering the detailed electronic structures of the clusters, based on the experimental PES spectra and the symmetries of the cluster frontier orbitals. First, from the calculated wave functions, we find that all the cluster molecular orbitals are fairly delocalized. The orbital delocalization indicates the sensitivity of the electronic structure to minor geometric structure changes in the iron cluster (e.g., addition or subtraction of a single atom). If such a change results in a change of the nature of the frontier orbitals, one expects that a cluster chemical reactivity change will follow. As described above, the behavior of the HOMOs in the iron clusters varies with cluster size as revealed from the EHMO wave functions, as well as from the PES spectral changes. This will naturally lead to different cluster reactivity. More specifically, when H_2 approaches a cluster, the effective orbital overlap between the H_2 σ^* and the HOMO of the cluster is critical in determining the reactivity. In general, two factors will influence this orbital interaction; the energy level and the symmetry of the cluster HOMOs. It is thus not surprising to find a correlation between the IP and the reactivity[9] because the IP is a measure of the HOMO levels. However, the HOMO energy level change in the cluster size range of interest is relatively small.[24] In fact, the IP change is less than 0.1 eV from Fe_{15} to Fe_{16} and less than 0.25 eV from Fe_{18} to Fe_{19}, while the reactivity changes by orders of magnitude in the same size ranges. The HOMO energy level match, therefore, is probably not the major effect in these cases. Siegbahn *et al.* arrived at the same conclusion.[28] Thus, the symmetry of the cluster HOMOs becomes the dominating factor in determining the orbital overlap—hence the reactivity. We believe this provides the key insight into the dramatically different reactivity with H_2 observed for the iron clusters.

As mentioned in Sec. IV, the HOMO levels, including those levels responsible for the sharp features in the spectra of Fe_{9-15}^- and those levels responsible for the second band in Fe_{16}^-, are mainly of $3d$ characters with large contributions from the central atom. The symmetry of these HOMOs matches with the H_2 σ^* orbital, leading to high reactivity. However, the HOMO of Fe_{16}^-, corresponding to the threshold feature in its PES spectrum, is distinctly different; it mainly has $4s$ characters with minor $3d$ contributions. It is not symmetry-matched with the H_2 σ^* orbital, hence an extremely low reactivity. The s-type HOMO of Fe_{16} provides a ''shielding effect'' to protect the cluster from being attacked by the incoming H_2 molecule despite the presence of the symmetry-matched d-type orbitals corresponding to the sec-

ond band in the PES spectrum. This will lead to a high activation barrier for the reaction. There is about a factor of 20 difference in the reactivity with H_2 between Fe_{15} and Fe_{16}.

From Fe_{16} to Fe_{18}, the HOMOs of the clusters are all nondegenerate and are mainly composed of *s* orbitals. Furthermore, the HOMO energy spacing to the next occupied level is fairly apart. Therefore, the reactivity of these clusters remains low. At Fe_{19}, the HOMO becomes twofold degenerate, due to the high symmetry of the cluster. It has four atoms arranged around an apex atom of the bcc Fe_{15} core, as shown in Fig. 9. Although these two orbitals are still composed mostly of *s* orbitals with substantial *d* contributions, they can readily recombine to form symmetry-matched molecular orbitals with the H_2 σ^* orbital. Therefore, it should exhibit a very different reactivity, compared to Fe_{18}. This is indeed what is observed in the experiment, that shows a reactivity increase of nearly 60 times in Fe_{19}.

From Fe_{20} to Fe_{24}, the calculated results suggest that there are more energy levels near the HOMOs, whose *d* components continue to increase as the cluster size increases. They become increasingly easy to form symmetry-matched frontier orbitals to the σ^* orbital of the incoming H_2 molecule. One thus observes sustained high reactivity in this size range. In particular, at Fe_{23}, the HOMO once again becomes twofold degenerate due to a higher symmetry of this cluster as shown in Fig. 10. This results in another reactivity jump in Fe_{23} over Fe_{22}.

In the above, we give a detailed microscopic interpretation of the dramatic size dependence of the iron cluster reactivity with H_2, based on the cluster electronic structure. Finally, we offer the following comments on the seemingly natural correlation between the high structural symmetry and high reactivity. Initially, the structural symmetry seems to be a dominant effect in determining the reactivity. This is observed in the cases of Fe_{15}, Fe_{19}, and Fe_{23}, which all possess high geometric symmetry with abruptly high reactivity. However, all clusters beyond Fe_{19} have high reactivity with H_2, while they do not necessarily possess high structural symmetries. The EHMO calculations show that the ultimate origin lies in the electronic structure of these clusters. Nevertheless, the high geometric symmetry often leads to high degree of degeneracy. The degenerate or near-degenerate HOMOs can be recombined to form symmetry-matched orbitals to interact effectively with the H_2 σ^*, which subsequently results in high reactivity.

VI. SUMMARY

An improved magnetic bottle time-of-flight photoelectron spectrometer is described for the study of the electronic structures for a wide variety of clusters. The 30 meV resolution achieved is no longer limited by the Doppler broadening due to the implementation of a momentum deceleration for the cluster beam. Thus, further improvement on the spectrometer resolution is possible.[53]

The PES spectra of small iron clusters, Fe_{3-24}^-, are presented, and the data are interpreted with the help of EHMO calculations. This is the first attempt to experimentally probe the iron cluster electronic structures. Small clusters from Fe_3 to Fe_8 show rather well resolved features. The spectra of Fe_3^- and Fe_4^- can be interpreted well by assuming equilateral triangular and tetrahedral structures, respectively, and both should be Jahn–Teller active. The spectra of Fe_{5-8}^- cannot be interpreted in detail from the EHMO calculations and high level calculations are required. Both Fe_6^- and Fe_7^- show rather diffuse spectra and both yield unusually low electron affinities. Sharp spectral features are observed for larger clusters. For Fe_{9-15}^-, the spectra are quite similar all with a sharp feature at the threshold. The EHMO results agree quite well with the PES spectra when bcc structures are assumed for these clusters. The spectrum of Fe_{16}^- is quite different from that of Fe_{15}^- and an extra feature appears at the threshold, suggesting the start of a new shell in the cluster growth. Both Fe_{17}^- and Fe_{18}^- have similar spectra as Fe_{16}^-, with increasing intensity for the extra feature. At Fe_{19}^-, this extra feature becomes a well resolved peak and the spectrum shifts to a lower binding energy. This pattern of change from Fe_{16}^- to Fe_{19}^- is repeated from Fe_{20}^- to Fe_{23}^-. All these PES spectral changes coincide with the chemical reactivity changes (with H_2) occurring in the same cluster sizes. The EHMO calculations, by assuming close-packed structures with a bcc Fe_{15} core, are in reasonable agreement with the spectra, in particular, for Fe_{16}^-. From the symmetry of the HOMO levels of the clusters and the PES spectral changes, a detailed microscopic explanation of the dramatic cluster size-dependent reactivity with H_2 is proposed. The EHMO calculations also correctly predict the existence of magnetism in these clusters. The electronic and structural properties of these iron clusters are interesting and it would be desirable to confirm these conclusions by using high level theories.

ACKNOWLEDGMENTS

L.S.W. gratefully acknowledges Dr. L. Bloomfield, Dr. O. Cheshnovsky, Dr. D. Ray, and Dr. R. E. Smalley for various helpful discussions about the instrument and Dr. S. D. Colson and Dr. L. Lou for valuable discussions of this work. H.S.C. would like to acknowledge Dr. P. M. Mathias and Dr. G. P. Pez for their critical reading of the manuscript. He is also grateful to Professor M.-H. Whangbo for providing the extended Hückel program and to Dr. J. Ren for valuable discussions. We thank Pacific Northwest Laboratory and the U.S. Department of Energy, Basic Energy Sciences for the development of the cluster PES apparatus. Support for the study of transition metal clusters from the National Science Foundation (Grant No. CHE-9404428) is gratefully acknowledged. This work was performed at Pacific Northwest Laboratory, a multiprogram national laboratory operated for the U.S. Department of Energy by Battelle Memorial Institute under Contract No. DE-AC06-76RLO 1830.

[1] See, for example, *Physics and Chemistry of Finite Systems: From Clusters to Crystals*, edited by P. Jena, S. N. Khanna, and B. K. Rao (Kluwer Academic, Boston, 1992), Vols. I and II.
[2] I. M. L. Billas, A. Chatelain, and W. A. de Heer, Science **265**, 1682 (1994).
[3] D. M. Cox, D. J. Trevor, R. L. Whetten, E. A. Rohlfing, and A. Kaldor, Phys. Rev. B **32**, 7290 (1985).
[4] W. A. de Heer, P. Milani, and A. Chatelain, Phys. Rev. Lett. **65**, 488 (1990).
[5] J. P. Bucher, D. C. Douglass, and L. A. Bloomfield, Phys. Rev. Lett. **66**, 3052 (1991).

[6] M. E. Geusic, M. D. Morse, and R. E. Smalley, J. Chem. Phys. **82**, 590 (1985).
[7] M. D. Morse, M. E. Geusic, J. R. Heath, and R. E. Smalley, J. Chem. Phys. **83**, 2293 (1985).
[8] S. C. Richtsmeier, E. K. Parks, K. Liu, L. G. Pobo, and S. J. Riley, J. Chem. Phys. **82**, 3659 (1985).
[9] R. L. Whetten, D. M. Cox, D. J. Trevor, and A. Kaldor, Phys. Rev. Lett. **54**, 1494 (1985).
[10] E. K. Parks, K. Liu, S. C. Richtsmeier, L. G. Pobo, and S. J. Riley, J. Chem. Phys. **82**, 5470 (1985).
[11] P. J. Brucat, C. L. Pettiette, L. S. Zheng, M. J. Craycraft, and R. E. Smalley, J. Chem. Phys. **85**, 4747 (1986).
[12] E. K. Parks, B. H. Weiller, P. S. Bechthold, W. F. Hoffman, G. C. Nieman, L. G. Pobo, and S. J. Riley, J. Chem. Phys. **88**, 1622 (1988).
[13] D. M. Cox, K. C. Reichmann, D. J. Trevor, and A. Kaldor, J. Chem. Phys. **88**, 111 (1988).
[14] E. K. Parks, G. C. Nieman, L. G. Pobo, and S. J. Riley, J. Chem. Phys. **88**, 6260 (1988).
[15] J. Harris and R. O. Jones, J. Chem. Phys. **70**, 830 (1979).
[16] I. Shim and K. A. Gingerich, J. Chem. Phys. **77**, 2490 (1982).
[17] D. G. Leopold and W. C. Lineberger, J. Chem. Phys. **85**, 51 (1986).
[18] D. G. Leopold, J. Almlof, W. C. Lineberger, and P. R. Taylor, J. Chem. Phys. **88**, 3780 (1988).
[19] M. Tomonari and H. Tatewaki, J. Chem. Phys. **88**, 1828 (1988).
[20] T. Noro, C. Ballard, M. H. Palmer, and H. Tatewaki, J. Chem. Phys. **100**, 452 (1994).
[21] D. R. Salahub, in *Ab Initio Methods in Quantum Chemistry—II*, edited by K. P. Lawless (Wiley, New York, 1987).
[22] M. D. Morse, Chem. Rev. **86**, 1049 (1986).
[23] J. Koutecky and P. Fantucci, Chem. Rev. **86**, 539 (1986).
[24] S. Yang and M. B. Knickelbein, J. Chem. Phys. **93**, 1533 (1990).
[25] E. K. Parks, T. D. Klots, and S. J. Riley, J. Chem. Phys. **92**, 3813 (1990).
[26] E. A. Rohlfing, D. M. Cox, A. Kaldor, and K. H. Johnson, J. Chem. Phys. **81**, 3846 (1984).
[27] L. Lian, C. X. Su, and P. B. Armentrout, J. Chem. Phys. **97**, 4072 (1992).
[28] I. Panas, P. Siegbahn, and U. Wahlgren, in *The Challenge of d and f Electrons* (American Chemical Society, Washington, D.C., 1989), p. 125.
[29] J. Conceicao, R. T. Laaksonen, L. S. Wang, T. Guo, P. Nordlander, and R. E. Smalley, Phys. Rev. B **51**, 4668 (1995).
[30] C. Y. Yang, K. H. Johnson, D. R. Salahub, J. Kaspar, and R. P. Messmer, Phys. Rev. B **24**, 5673 (1981).
[31] K. Lee, J. Callaway, and S. Dhar, Phys. Rev. B **30**, 1724 (1984).
[32] G. F. Holland, D. E. Ellis, and W. C. Trogler, J. Chem. Phys. **83**, 3507 (1985).
[33] G. M. Pastor, J. Dorantes-Davila, and K. H. Bennemann, Chem. Phys. Lett. **148**, 459 (1988).
[34] G. M. Pastor, J. Dorantes-Davila, and K. H. Bennemann, Phys. Rev. B **40**, 7642 (1989).
[35] J. L. Chen, C. S. Wang, K. A. Jackson, and M. R. Pederson, Phys. Rev. B **44**, 6558 (1991).
[36] M. Castro and D. R. Salahub, Phys. Rev. B **47**, 10 955 (1993).
[37] D. G. Leopold, J. Ho, and W. C. Lineberger, J. Chem. Phys. **86**, 1715 (1987).
[38] O. Cheshnovsky, S. H. Yang, C. L. Pettiette, M. J. Craycraft, and R. E. Smalley, Rev. Sci. Instrum. **58**, 2131 (1987).
[39] G. Gantefor, K. H. Meiwes-Broer, and H. O. Lutz, Phys. Rev. A **37**, 2716 (1988).
[40] K. M. McHugh, J. G. Eaton, G. H. Lee, H. W. Sarkas, L. H. Kidder, J. T. Snodgrass, M. R. Manaa, and K. H. Bowen, J. Chem. Phys. **91**, 3792 (1989).
[41] K. Rademann, Ber. Bunsenges. Phys. Chem. **93**, 653 (1989).
[42] T. N. Kitsopoulos, C. J. Chick, Y. Zhao, and D. M. Neumark, J. Chem. Phys. **95**, 1441 (1991).
[43] C.-Y. Cha, G. Gantefor, and W. Eberhardt, Rev. Sci. Instrum. **63**, 5661 (1992).
[44] P. Kruit and F. H. Read, J. Phys. E **16**, 313 (1983).
[45] J. Fan and L. S. Wang, J. Phys. Chem. **98**, 11 814 (1994).
[46] J. Fan, L. Lou, and L. S. Wang, J. Chem. Phys. **102**, 2701 (1995).
[47] L. S. Wang, Surf. Rev. Lett. (to be published).
[48] L. S. Wang, J. Fan, and L. Lou, Surf. Rev. Lett. (to be published).
[49] L. S. Wang, J. Conceicao, C. Jin, and R. E. Smalley, Chem. Phys. Lett. **182**, 5 (1991).
[50] W. A. de Heer and P. Milani, Rev. Sci. Instrum. **62**, 670 (1991).
[51] (a) G. Markovich, R. Giniger, M. Levin, and O. Cheshnovsky, J. Chem. Phys. **95**, 9416 (1991); (b) G. Markovich, S. Pollack, R. Giniger, and O. Cheshnovsky, *ibid*. **101**, 9344 (1994).
[52] C. E. Moore, *Atomic Energy Levels*, Natl. Bur. Stand. Circ. (U.S. GPO, Washington, D.C., 1971), Vol. II.
[53] L. S. Wang, J. Fan, and H. Wu (unpublished).
[54] Y. Wang, T. F. George, D. M. Lindsay, and A. C. Beri, J. Chem. Phys. **86**, 3493 (1987).
[55] D. M. Lindsay, Y. Wang, and T. F. George, J. Chem. Phys. **86**, 3500 (1987).
[56] A. Yoshida, T. Dossing, and M. Manninen, J. Chem. Phys. **101**, 3041 (1994).
[57] R. Hoffmann, J. Chem. Phys. **39**, 1397 (1963).
[58] J. V. Saillard and R. Hoffmann, J. Am. Chem. Soc. **106**, 2006 (1984).
[59] R. Hoffmann, Rev. Mod. Phys. **60**, 601 (1988).
[60] E. Canadell and M.-H. Whangbo, Chem. Rev. **91**, 965 (1991).
[61] S. L. Dixon and P. C. Jurs, J. Comput. Chem. **15**, 733 (1994).
[62] E. K. Parks, B. J. Winter, T. D. Klots, and S. J. Riley, J. Chem. Phys. **96**, 8267 (1992).
[63] E. K. Parks and S. J. Riley, J. Chem. Phys. **99**, 5898 (1993).
[64] O. B. Christensen and M. L. Cohen, Phys. Rev. B **47**, 13 643 (1993).
[65] W. A. Harrison, *Electronic Structure and the Properties of Solids—The Physics of the Chemical Bond* (Freeman, San Francisco, 1980).
[66] In the extended Hückel theory, the extra electron in the anion does not alter the energy level structure of the cluster; it enters the lowest energy, singly occupied level.
[67] L. S. Wang, H. S. Cheng, and J. Fan, Chem. Phys. Lett. **236**, 57 (1995).
[68] J. Ho, M. L. Polak, K. M. Ervin, and W. C. Lineberger, J. Chem. Phys. **99**, 8542 (1993).
[69] K. M. Ervin, J. Ho, and W. C. Lineberger, J. Chem. Phys. **89**, 4514 (1988).
[70] J. Zhao, X. Chen, and G. Wang, Phys. Rev. B **50**, 15 424 (1994).